Supporting Information Available

Electrochemical measurements

The material reaches relatively stable cycling conditions after three cycles. All cycles measured for Figure 1, i.e. CVs with different lower vertices, are shown in Figure 9.

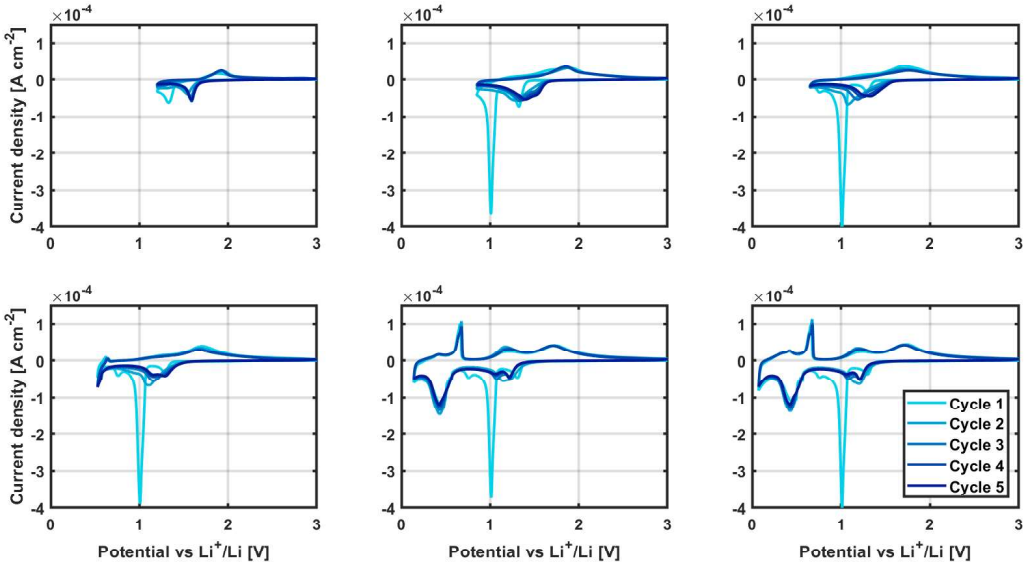

Figure 9: First five cycles of a CV conducted on a 20 nm ITO film showing the activation process in the first cycle and subsequent stabilization of the material using a lower vertex of 1.2 V, 0.85 V, 0.65 V, 0.53 V, 0.14 V, en 0.075 V.

Measurement of electronic conductivity

Four point probe measurements are executed on ITO films of different thicknesses. The sheet resistance is measured as a function of the applied potential for each thickness. Figure 10 shows the results of these measurements. No correlation between the applied potential and sheet resistance is observed. A clear linear relation between the inverse of sheet resistance and layer thickness is observed. The film resistivity is calculated by fitting this trend, yielding a value of 6.22 $10^{-4}\Omega \cdot$cm.

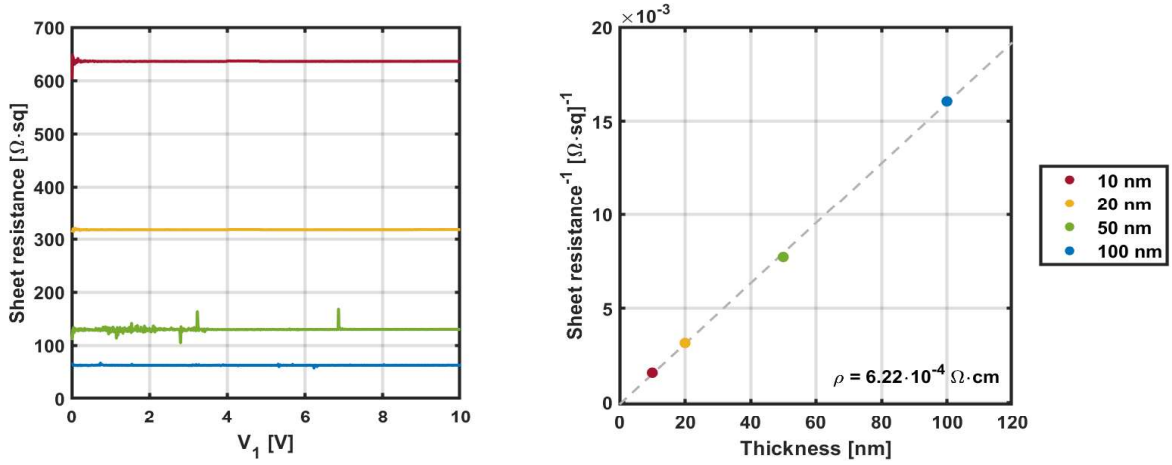

Figure 10: Raw data of the sheet resistance measurement conducted on 10 nm, 20 nm, 50 nm, and 100 nm thick ITO films.

The set-up used to study the conductivity of ITO as a function of the lithiation state is shown in figure 11. Panel (a) illustrates the cell configuration used to lithiate and delithiate the ITO film. In this case, the two gold contacts are short circuited to function as a current collector for ITO, and lithium strips are inserted into the vertical compartments as reference and counter electrodes. Panel (b) is a schematic of the top view of the sample. Two gold islands are deposited on top of a SiO_2 substrate. These islands are spaced 2600 μm apart. ITO is deposited over the gap, contact both gold pads. To measure the conductivity at a certain state of lithiation, the gold pads are connected independently as counter/reference and working electrode in a two-electrode configuration.

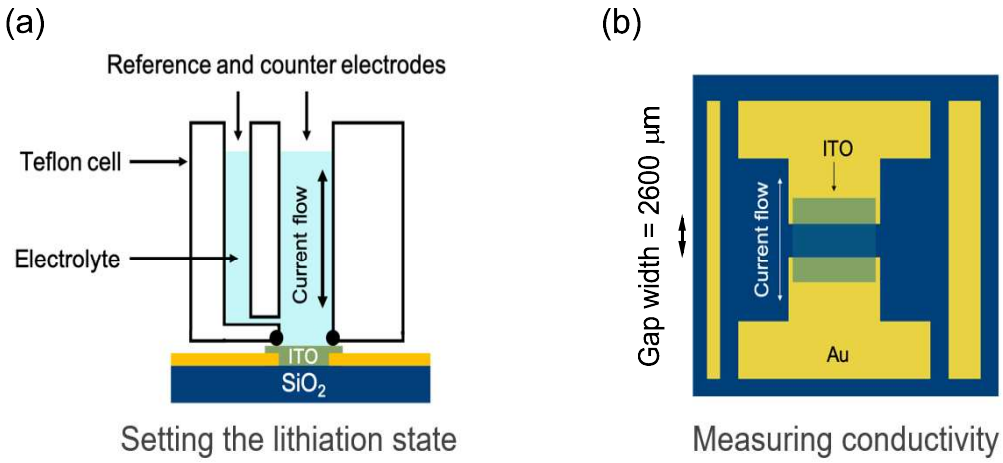

Figure 11: Lay-out of the test set-up used to determine the changes in electronic conductivity at different lithition conditions. (a) depicts the configuration used to set the lithiation state of the ITO, (b) shows a top view schematic of the current collector.

In the main paper the shown conductivity values are the average of a 10 nm and a 20 nm sample. The measured conductivity for the separate samples is shown in figure 12 below.

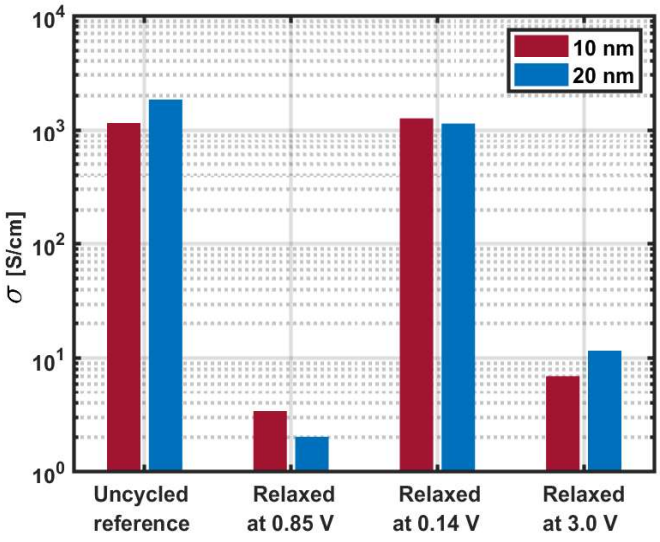

Figure 12: Electronic conductivity of ITO as a function of lithiation state measured in a 10 nm and 20 nm ITO film.

Physical characterization of ITO

Ellipsometry is used to calibrate the deposition rate of the sputter process. Figure 13 below shows this thickness calibration. The deposition rate was determined to be 0.313 nm/s.

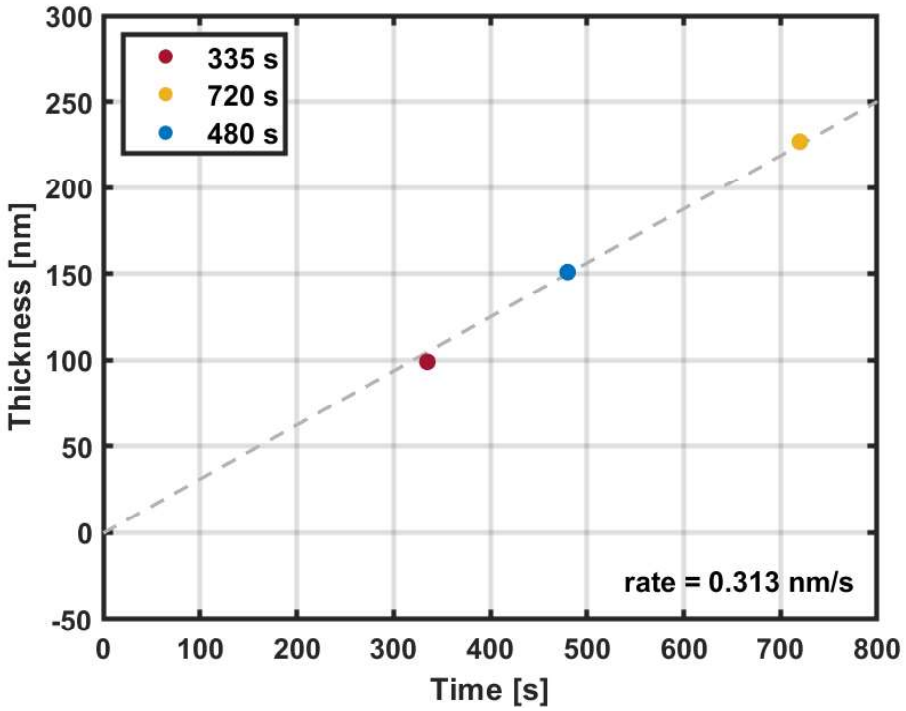

Figure 13: Growth rate of the RF sputtered ITO film, as measured using ellipsometry.

ITO films are deposited on TiN substrates for physical characterizations. The raw data of the ERD measurements in figure 7 is shown in figure 14. The top figures show the raw data collected on as-deposited ITO, the bottom figures show the results after a full cycle. The left figures show time-of-flight data with a characteristic banana shape, the figures on the right show the data after conversion to isotopic masses.

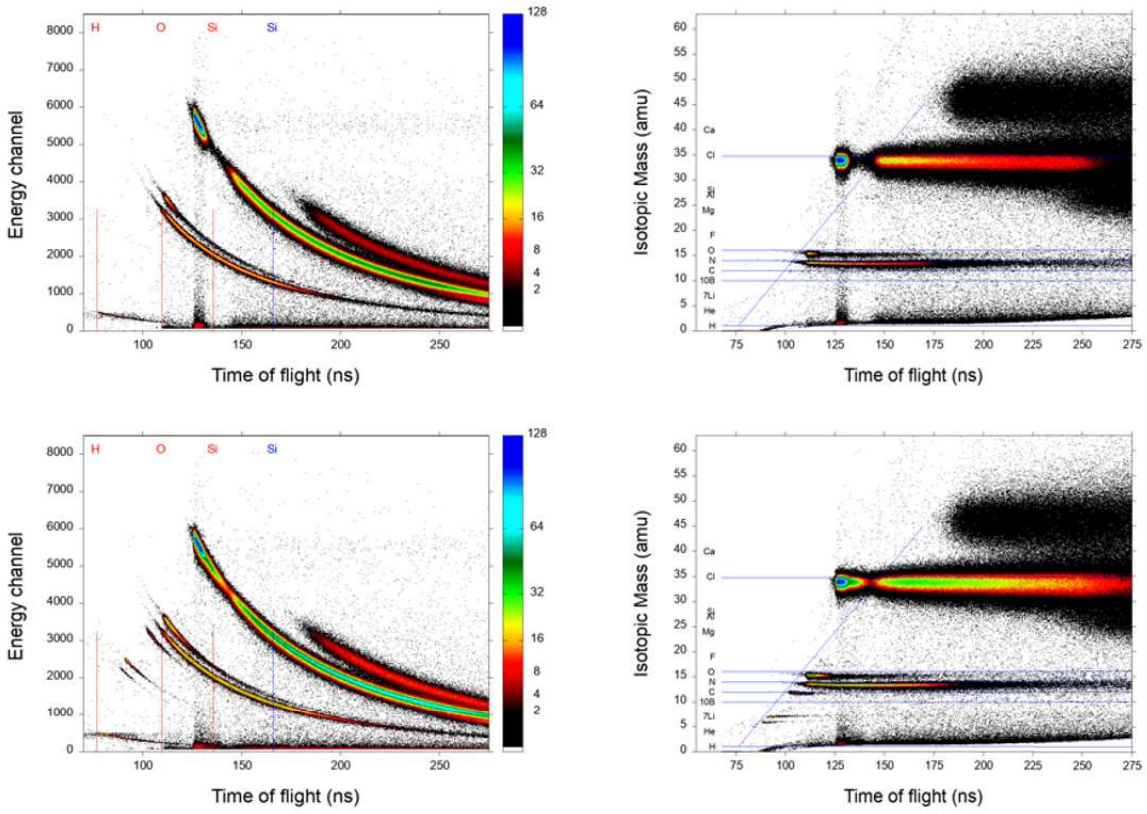

Figure 14: Raw data of the as-deposited (top) and cycled (bottom) ITO sample.

The atomic concentration of each element determined from these ERD measurements is given in table 2. Here, M is used to indicate the sum of the In and Sn concentrations. The concentrations are calculated from results in the slab regions indicated by the dashed lines in figure 7. The absolute uncertainty on this measurement is 2 at% for the majority constituents, i.e. those elements with atomic fractions exceeding 15 at%. For elements with an atomic fraction below 7%, the uncertainty is 0.7%.

Table 2: Atomic concentrations calculated from ERD measurements on an as-deposited ITO film and a cycled film.

Compositional analysis ITO on TiN			
As-deposited		**Cycled**	
H :	3.4%	**H :**	13.6%
Li:	0.0%	**Li:**	13.3%
C :	0.0%	**C :**	5.4%
O :	57.0%	**O :**	46.7%
M	39.6%	**M**	21.0%

The raw data of the RBS and PIXE measurements are shown in figures 15 and 16, respectively. The RBS analysis is performed using software developed in-house called "SA-numeric integration". Based on the results from numeric integration, plots have been generated using this software. The PIXE spectra are analyzed using the GupixWin software. The two fitted models are displayed below.

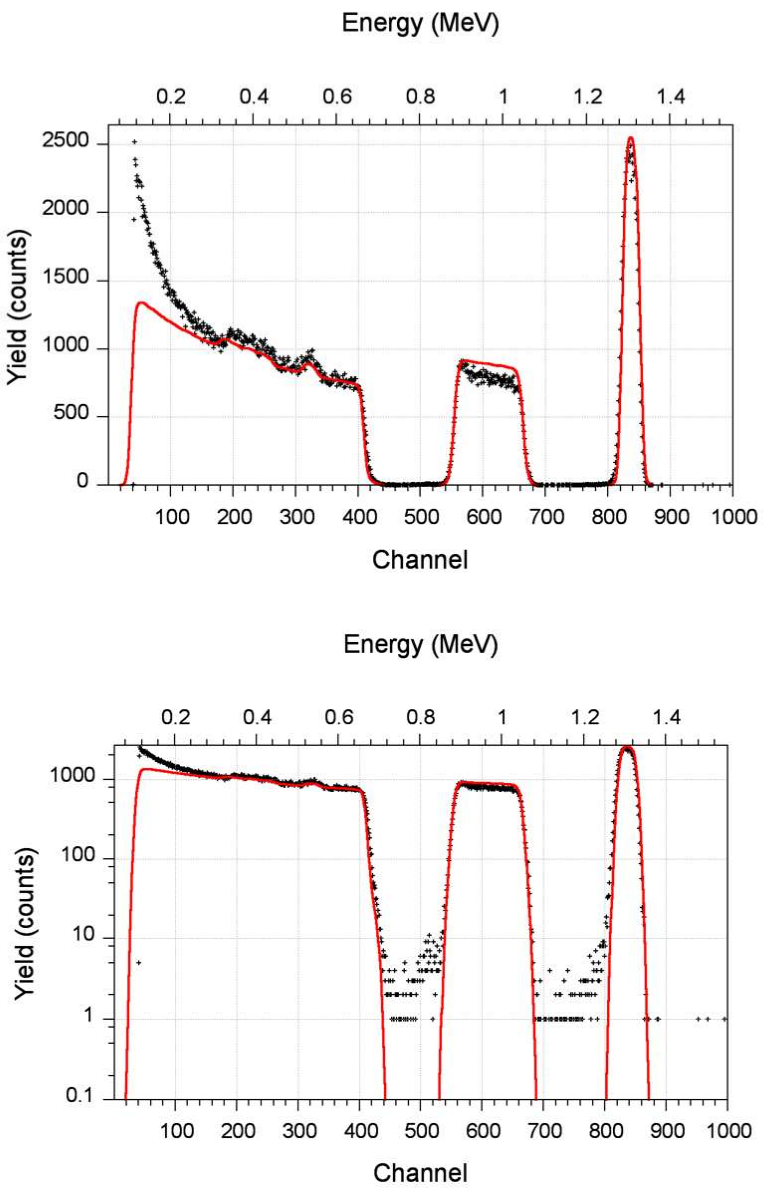

Figure 15: Raw data of the RBS measurement. The fitted model is indicated with the red line.

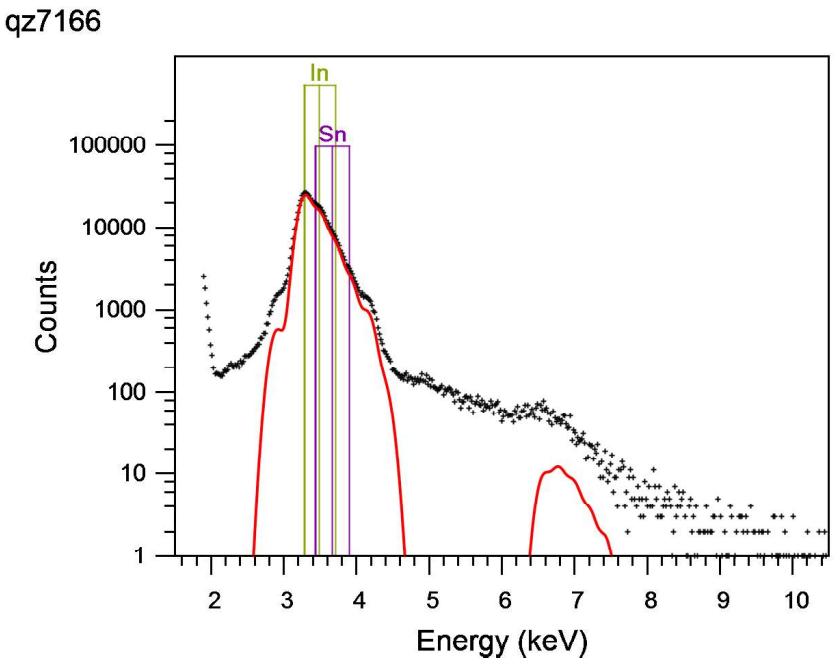

Figure 16: Raw data of the PIXE measurement. The fitted model is indicated with the red line.

All elemental distributions measured using EDX are shown in figure 17.

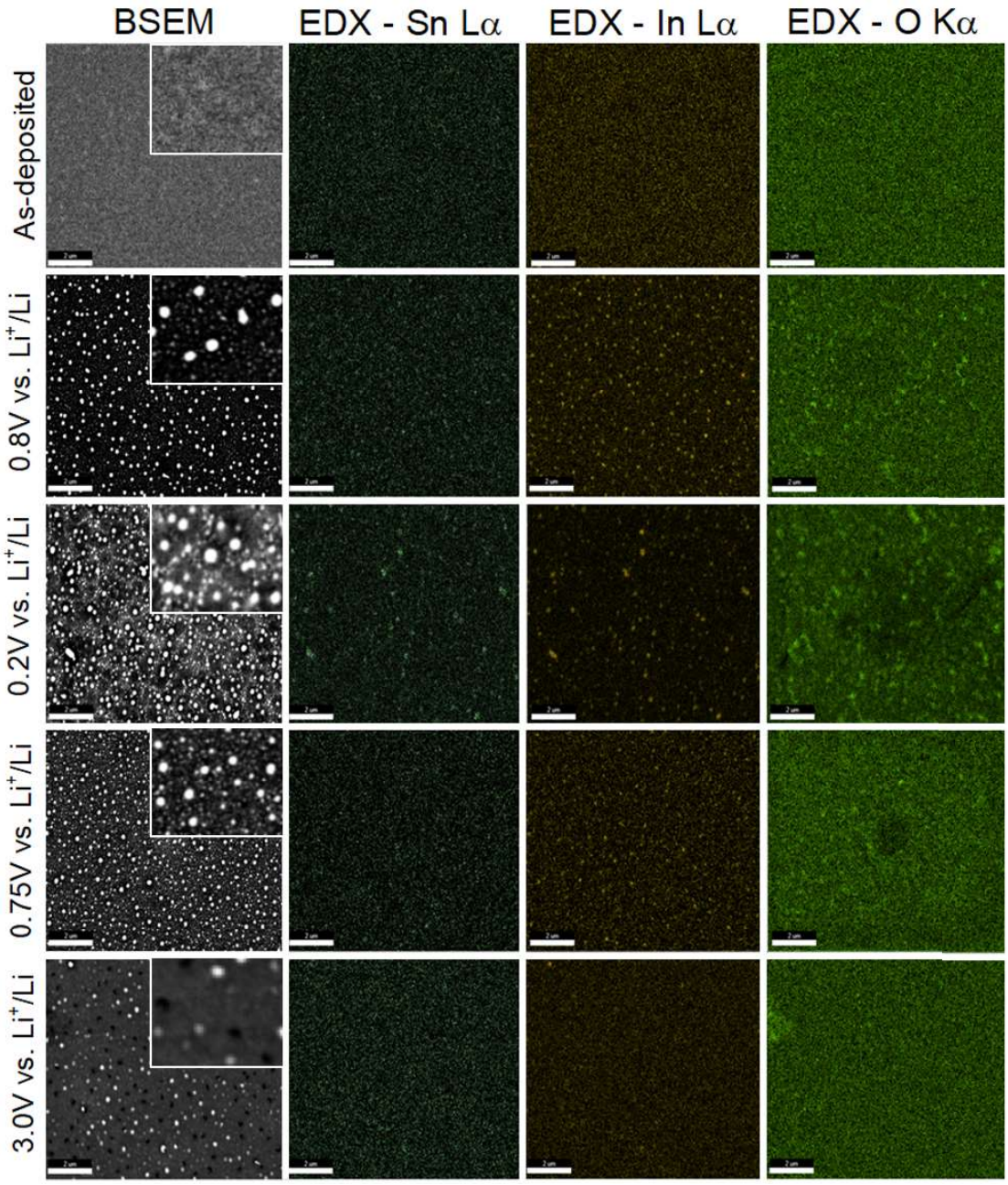

Figure 17: Elemental maps at different stages of lithiation.

The raw XPS data is provided in Figures 18-20. In and Sn are still detected on samples cycled to 1.2 V, 0.75 V, and 3 V - however, the presence of the carbon-containing layer on top of ITO results in lower detected concentrations. The formation of this carbonate layer is so severe on the samples lithiated to 0.8 V and 0.2 V that only the carbon, lithium and oxygen from the top layer and carbon contamination due to air exposure are detected. No

differences in oxidation state of either In or Sn can be deduced from the XPS measurement. The $In2p^3$ peak position and shape is similar for all samples for which this peak is observed, as In and Sn change their oxidation state, the shift in the $In2p^3$ and $Sn2p^3$ remain minor.

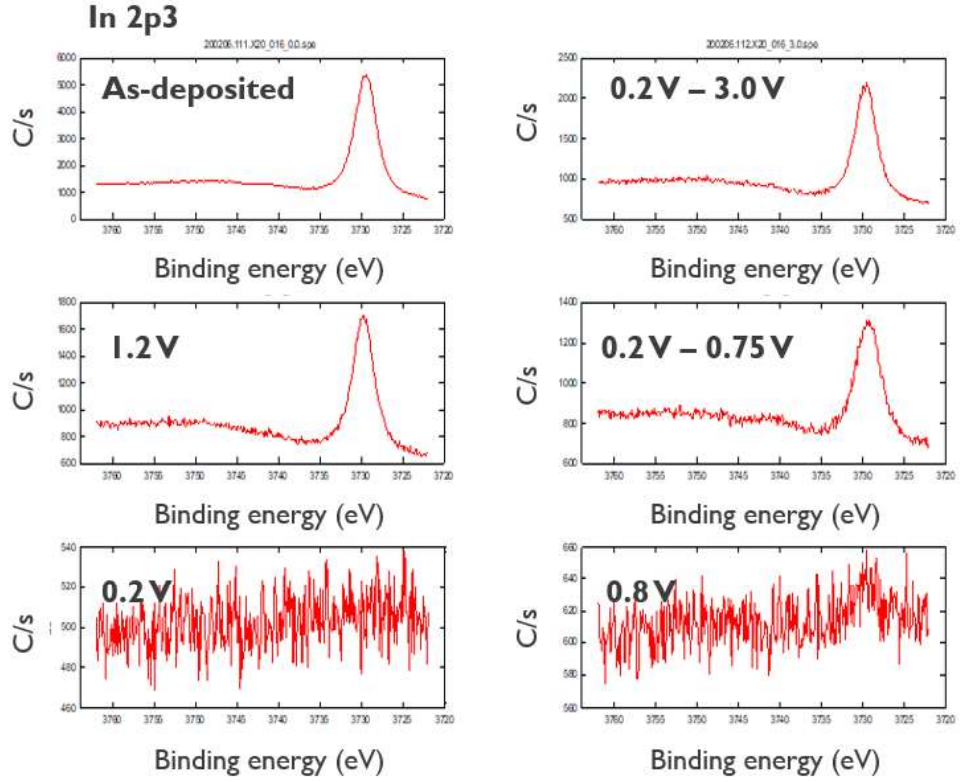

Figure 18: In 2p3 specta measured on ITO films equilibrated at different potentials.

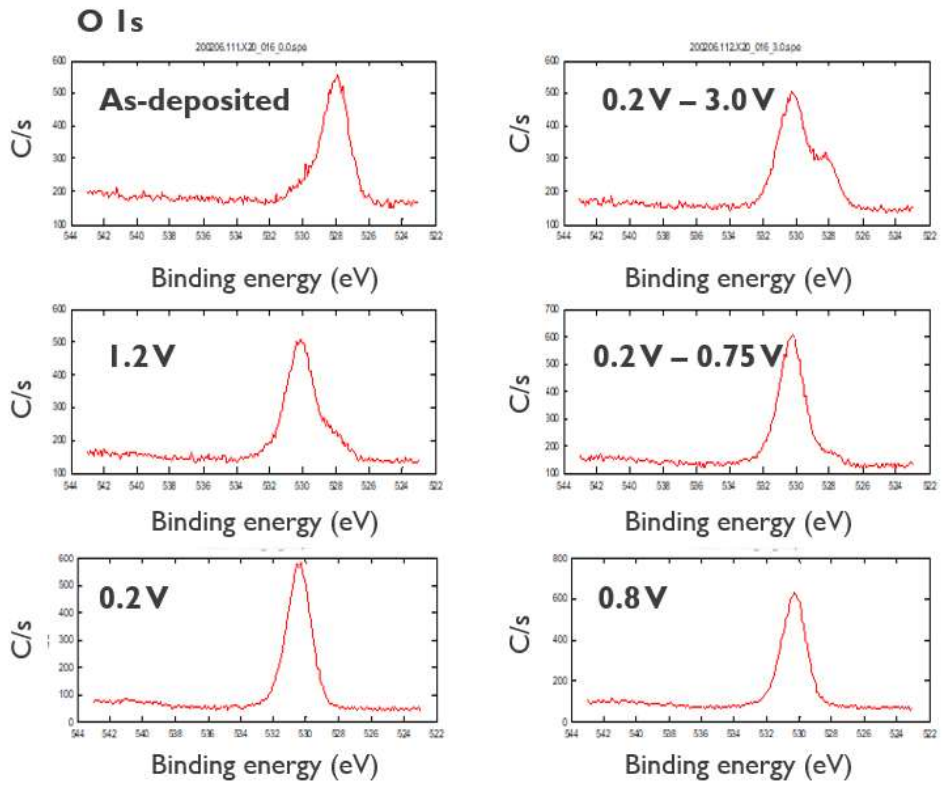

Figure 19: O 1s specta measured on ITO films equilibrated at different potentials.

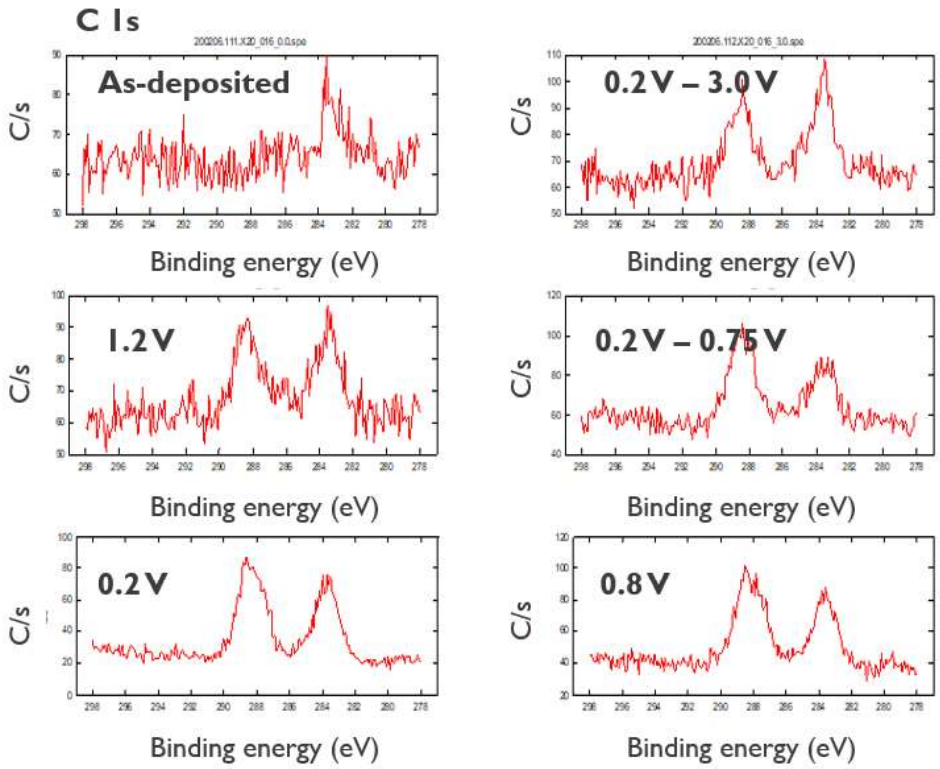

Figure 20: C 1s specta measured on ITO films equilibrated at different potentials.